bioRxiv preprint doi: https://doi.org/10.1101/538165; this version posted February 1, 2019. The copyright holder for this preprint (which was not certified by peer review) is the author/funder, who has granted bioRxiv a license to display the preprint in perpetuity. It is made available under aCC-BY-NC-ND 4.0 International license.

A Stomata Classification and Detection System in Microscope Images of Maize Cultivars

Alexandre H. Aono[a], James S. Nagai[a], Gabriella da S. M. Dickel[b], Rafaela C. Marinho[b], Paulo E. A. M. de Oliveira[b], Fabio A. Faria[a,*]

[a] *Instituto de Ciêcia e Tecnologia, Universidade Federal de São Paulo – UNIFESP*
12247-014, São José dos Campos, SP – Brazil
[b] *Instituto de Biologia, Universidade Federal de Uberlândia*
Uberlndia, MG, Brazil

Abstract

Stomata are morphological structures of plants that have been receiving constant attention. These pores are responsible for the interaction between the internal plant system and the environment, working on different processes such as photosynthesis process and transpiration stream. As evaluated before, understanding the pore mechanism play a key role to explore the evolution and behavior of plants. Although the study of stomata in dicots species of plants have advanced, there is little information about stomata of cereal grasses. In addition, automated detection of these structures have been presented on the literature, but some gaps are still uncovered. This fact is motivated by high morphological variation of stomata and the presence of noise from the image acquisition step. Herein, we propose a new methodology of an automatic stomata classification and detection system in microscope images for maize cultivars. In our experiments, we have achieved an approximated accuracy of 97.1% in the identification of stomata regions using classifiers based on deep learning features.

Keywords: deep learning, image classification, pattern recognition.

1. Introduction

According to Willmer and Fricker [1], from all points of view, the stomata have received more constant attention probably than any other single vegetative structure in the plant. Regulating gas exchange between the plant and the environment[2], these structures are small pores on the surfaces of leaves, stems and parts of angiosperm flowers and fruits [3, 4], formed by a pair of specialized epidermal cells (guarder cells), which are found in the surface of aerial parts of most higher plants [1]. Due to the controlling of the exchange of water vapour and CO^2 between the interior of the leaf and the atmosphere [3]; the photosynthesis, the transpiration stream, the nutrition and the metabolism of land plants are in different ways related to the opening and closing movements of the stomata [4, 1]. Furthermore, Hetherington and Woodward point that the acquisition of stomata and an impervious leaf cuticle are considered to be key elements in the evolution of advanced terrestrial plants, allowing the plant to inhabit a range of different, often fluctuating environments but still control water content [3].

The stomatal movements distinguish this structure from other pores found in plant organs, as for example, pneumathodes, hydathodes, lenticels, and the breathing pores found in the thalli

*Corresponding author: Tel.: +55 (12) 3309-9500; fax: +55 (12) 3921-8857;
Email address: ffaria@ic.unicamp.br (Fabio A. Faria)

bioRxiv preprint doi: https://doi.org/10.1101/538165; this version posted February 1, 2019. The copyright holder for this preprint (which was not certified by peer review) is the author/funder, who has granted bioRxiv a license to display the preprint in perpetuity. It is made available under aCC-BY-NC-ND 4.0 International license.

of liverworts [1]. The control of stomatal aperture requires the coordinated control of multiple cellular processes [3] and its morphogenesis is affected by several environmental stimuli, such as relative humidity, temperature, concentration of atmospheric carbon dioxide, light intensity, and endogenous plant hormones [2, 3, 1]. Global warming for example could increase leaf transpiration and soil evaporation, and as consequence leaf stomata movements can control plant water loss and carbon gain under this water stress condition [5]. Stomatal aperture might also represent an initial response to both plants and human pathogenic bacteria [2]. In plants, it has been reported that microscopic surface openings serve as passive ports of bacterial entry during infection and the stomatal closure is part of a plant innate immune response to restrict bacterial invasion [6].

The number of pores per unit area varies not only between species but also within species because of the influence of environmental factors during growth, leaf morphology and genetic composition [4, 1]. In general, it happens due to the influence on cell size [4], e.g. smaller guarder cells are usually associated with higher stomatal frequencies [1]. Besides stomata differentiation is a process that occurs together with the development of plant organs and, therefore, counts of stomata per unit area carried out at different stages in leaf development will differ [4]. Another characteristic with great variation is the spacing of stomata, which may be fairly evenly spaced throughout a leaf, located in regular rows along the length of a leaf, or they may be clustered in patches [1].

In view of the considerations above, the types of stomatal configuration are highly different. The study and identification of these pores are key points to understand several mechanisms of plants. Haworth et al. [7] also state that it may be reasonable to assume that stomatal structures have played a significant role in plant evolution over the last 400 million years. Nevertheless, the examination of stomata from microscope images involves manual measurement and is highly dependent on biologists with expert knowledge to correctly identify and measure stomatal morphology [8].

Even with the clear relevance of these structures, a recent study [9] indicated that surprisingly we still know little about stomata of cereal grasses. These grasses are extremely important, because they provide the majority of calories consumed by humans either directly through the consumption of grains or indirectly through animals fed a diet of grains and forage[10].

As pointed by [9], the stomatal complexes in grasses differ of the dicots in many ways, e.g. the guard cells of dicots are kidney-shaped and form stomata that are scattered throughout the epidermis in a less orderly pattern, while stomatal configuration of grasses develop in parallel rows within defined and specific epidermal cell files [9]. Herein we selected microscope images of maize, which represent the most produced and consumed cultivars in the world.

In this scenario, in order to assist the biological community to perform stomata studies, we develop an automated strategy for stomata detection in microscope images. The introduction of such techniques in these analyses represent a less time consuming way of examining stomatal behavior, enabling biologists to use more data-points from the images and study a broader range of stomata.

2. Related Work

This section presents some works concerned on stomata identification using image processing techniques.

The research of stomata image processing started in the 80s. Recognized as possible pioneers, Omasa and Onoe [11] proposed a technique for measuring stomata characteristics in gray scale images using Fourier Transform and threshold filters for image processing and segmenting [8].

bioRxiv preprint doi: https://doi.org/10.1101/538165; this version posted February 1, 2019. The copyright holder for this preprint (which was not certified by peer review) is the author/funder, who has granted bioRxiv a license to display the preprint in perpetuity. It is made available under aCC-BY-NC-ND 4.0 International license.

More recently, Sanyal et al. [12] compared tomato cultivars using several morphological characteristics, including stomata measures. Microscope images of different cultivars were obtained using a scanning electron microscope and the segmentation was performed using a watershed algorithm resulting in one stomata per image, followed by morphological operations (e.g., erosion and dilation) and Sorbel kernel filters to remove noise and obtain stomatal boundaries. Using 100 images of tomato cultivars and a multilayer perceptron algorithm, it was achieved 96.6% of accuracy.

In [13], a remote sensing processing was used to estimate stomata density. Three different regions of *Populus Euphratica* leaves were used as source of stomata images. For image processing, a object-oriented classification method was used with parameters such as scale, compactness and shape. This approach presented high accuracy when compared to human-based count, showing advantages over the traditional method to extract the stoma information [13].

Aiming the constant growth and development of stomata image processing studies, [14] published the Live Images of Plant Stomata LIPS database. In other work, [15] presented a semi-automatic stomata region detection using ImageJ software[16] and a Clustering-Aided Rapid Training Agent-based algorithm[17].

In an approach based solely on morphological operations[18], the authors developed a pipeline to count stomata. Initially, Gaussian low-pass filter was employed to preprocess the image and remove noise. In this sequence, reconstruction operations (e.g., opening and closing) were applied in order to highlight stomata regions. These pores were counted based on background intensity differences. As result, they presented a simplest approach to count stomata with mean precision of 94.3%.

In 2014, [19] presented a supervised method for stomata detection based on the measure of morphological and structural features. For this task, 24 microscope images were obtained and filtered by normalization together with a Gaussian filter. The stoma images were manually segmented and the width and height parameters extracted. The stomata detection procedure based on stomata morphological constraints achieved results close to a manual counting approach. With a similar procedure, a patent of stomata measurement using Gaussian filtering and morphological operations was registered [20].

Recently, Duarte et. al.[21] proposed a method to automatically count stomata in microscope images. Initially, the images were converted from RGB to CieLAB in order to select the best channel for analysis. The stomata detection was performed by Wavelet Spot Detection and morphological operations, and the watershed algorithm was used resulting in 90.6% of accuracy compared to non-automatic counting.

In the same year, [8] proposed an automated stomata detection and pore measurement for grapevines. This approach used a Cascade Object Detection (COD) algorithm with two main steps. First, the COD classifiers were trained using stoma and non-stoma images. Second, a slide window over the microscope images was used to identify stomata inside it. After its detection, the pore measurement step was performed using binary segmentation and skeletonization with ellipse fitting, estimating pore measurements for incomplete stoma. As a result the method proposed reached 91.6% of precision.

3. Proposed System

This section introduces the proposed stomata classification and detection system.

3.1. Overview

The proposed stomata classification and detection system is composed of two different process: (1) Stomata region classification; and (2) Stomata region detection.

bioRxiv preprint doi: https://doi.org/10.1101/538165; this version posted February 1, 2019. The copyright holder for this preprint (which was not certified by peer review) is the author/funder, who has granted bioRxiv a license to display the preprint in perpetuity. It is made available under aCC-BY-NC-ND 4.0 International license.

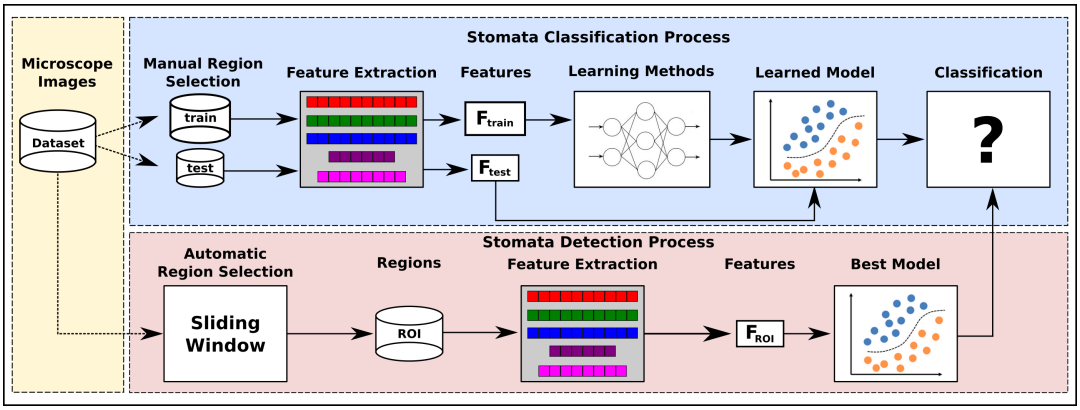

Figure 1: An overview of the stomata classification and detection system.

In the stomata classification process, the first step is to manually collect and label a subset of stomata and non-stomata regions from the microscope images dataset, creating two disjoint sets of subimages (*train* and *test*). These sets of subimages are subjected to an image descriptor that codes the visual properties of these subimages into feature vectors (F_{train} and F_{test}). Next, the feature vectors F_{train} are used as input for a learning method, creating a learned model for stomata classification task. Finally, each feature vector F_{test} is classified by this learned model. In the classification process, different image descriptors and learning methods are evaluated through a k-fold crossvalidation protocol and the best model is adopted to detect stomata regions on next process of proposed system.

In the stomata detection process, a sliding window is used on each microscope image from entire dataset, creating a set of regions of interest (ROI), which are subjected to an image descriptor resulting in the feature vectors (F_{ROI}) and finally, F_{ROI} are classified by the best model, i.e., a tuple (learning method + image descriptor) found in the classification process.

3.2. Stomata Classification Process

The first step for identifying stomata structures is the manual selection of a set of subimages containing stomata or other plant structures, labeled as non-stomata. Due to the differences between stomata size in distinct microscope images, we adopted a region/window of dimension 151×258 pixels, which was enough to include all of stomata regions in the available microscope images from dataset. Thus, a total of 1000 subimages of each class (stomata and non-stomata) have been selected to compose the new dataset.

Once the dataset has been created, the next step is to extract visual properties from the subimages using image descriptors. In this work, we evaluated eleven different image descriptors, DAISY, HOG, GIST, Haralick, LBP, and six deep learning-based descriptor (DenseNet121, InceptionResNetV2, InceptionV3, ModbileNet, NasNet and VGG16).

3.2.1. DAISY

DAISY descriptor relies on gradient orientation histograms. For an input image, orientation maps are calculated based on quantized directions. Each location (u, v) in a given map with a specific direction is equal to the image gradient norm (if its value is bigger than zero, else it is equal to zero). H orientation maps and several processes of convolution (using Gaussian kernels) are used to obtain convolved orientation maps. DAISY descriptor is the vector of values from these convolved maps located on concentric circles centered on a location, and where the amount of Gaussian smoothing is proportional to the radius of the circles [22].

bioRxiv preprint doi: https://doi.org/10.1101/538165; this version posted February 1, 2019. The copyright holder for this preprint (which was not certified by peer review) is the author/funder, who has granted bioRxiv a license to display the preprint in perpetuity. It is made available under aCC-BY-NC-ND 4.0 International license.

3.2.2. Histogram of Oriented Gradients (HOG)

Feature descriptor based on the creation of histograms with gradient orientation using its magnitude in localized portions of an image [23]. Local shape information is well described by the distribution of gradients in different orientations [24].

3.2.3. GIST

This descriptor has its focus on the shape of the scene itself, on the relationship between the outlines of the surfaces and their properties, ignoring the local objects in the scene and their relationships [25]. This approach does not require any form of segmentation and is based on a set of perceptual dimensions (naturalness, openness, roughness, expansion, ruggedness) [24].

3.2.4. Haralick Texture Features

As a first step, a gray-level co-occurrence matrix (GLCM) is constructed by considering the relation of each voxel with its neighborhood. Using different statistical measures (e.g., entropy, energy, variance, and correlation), texture properties are coded from the image into feature vectors [26].

3.2.5. Local Binary Patterns (LBP)

Computing a local representation of texture based on the comparison of each pixel with its neighborhood, a comparison threshold is defined and an output image is built with the binary to decimal values conversion and an histogram can be created [27].

3.2.6. Deep Convolutional Neural Network (DCNN)

A typical convolutional network is a fully-connected network where each hidden activation is computed by multiplying the entire input V by weights W in a given layer [28]. In this technique, a connection between traditional optimization-based schemes and a neural network architecture is used, where a separable structure is introduced as a reliable support for robust deconvolution against artifacts [29]. Once we do not have available a large scale of image to train a deep learning architecture from scratch, a good alternative is to use the transfer learning approach [30]. This approach uses deep learning architectures pre-trained with ImageNet dataset [31], adding other layers according to target application and then, the last layer can be used as a feature extraction function (image descriptor). In this work, we adopted six different architectures, DenseNet121 [32], InceptionResNetV2 [33], InceptionV3 [34], ModbileNet [35], NasNet [36] and VGG16 [37].

In this work, we used three different machine learning methods, Support Vector Machine [38] (SVM), Multilayer Perceptron [39] (MLP) and Adaboost [40] to evaluate the overall effectiveness results and to find the best learned model, i.e., a tuple (learning method + image descriptor) that will be adopted to label the new stomata regions on the next process.

Figure 2 shows the steps of the stomata classification process proposed in this work.

3.3. Stomata Detection Process

The methodology for detecting stomata regions is divided into the following steps as can be seen in image 4:

3.3.1. Dataset

A dataset with stoma and non-stoma subimages (see Figure 3) is created through a manual selection task from microscope images.

bioRxiv preprint doi: https://doi.org/10.1101/538165; this version posted February 1, 2019. The copyright holder for this preprint (which was not certified by peer review) is the author/funder, who has granted bioRxiv a license to display the preprint in perpetuity. It is made available under aCC-BY-NC-ND 4.0 International license.

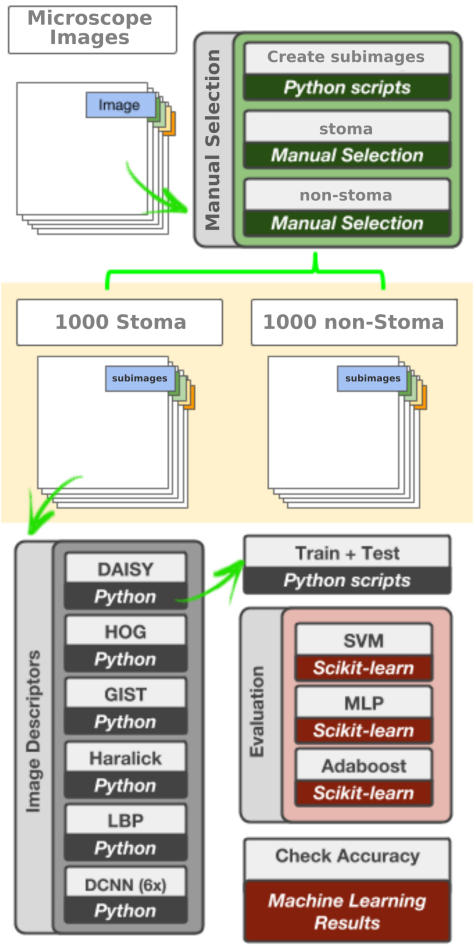

Figure 2: In-depth explanation of the stomata classification process.

3.3.2. Feature extraction

As the best descriptor has been found on the stomata classification process, the features of the created dataset are generated and stored into a table with the labels of each category (stoma or non-stoma).

3.3.3. Creation of the learned model

The descriptors were evaluated using three different learning methods, support vector machine (SVM), multi layer perceptron (MLP), and Adaboost. Based on the best effectiveness results achieved by learned model (a tuple composed of descriptor + learning method), the most appropriate learned model is selected to label the subimage in next step.

3.3.4. Sliding window iteration

Using a window of 151×258 pixels, an iteration over the microscope images is performed and for each generated subimage a label (stoma or non-stoma) is obtained using the best learned model. Due to the possible separation of stoma structures, the windows were created with a stride of 100 pixels in columns and rows.

3.3.5. Selection of positive regions

Based on the previous classification, an auxiliary matrix is filled in order to enable the posterior identification of stoma regions. Pixels with positive occurrence of stoma are separated from the rest of the image and the stoma regions can be analyzed.

bioRxiv preprint doi: https://doi.org/10.1101/538165; this version posted February 1, 2019. The copyright holder for this preprint (which was not certified by peer review) is the author/funder, who has granted bioRxiv a license to display the preprint in perpetuity. It is made available under aCC-BY-NC-ND 4.0 International license.

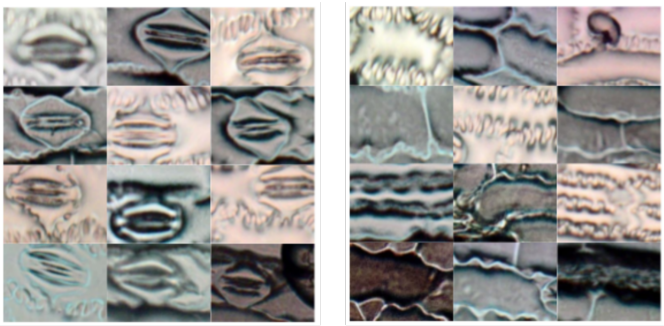

(a) (b)

Figure 3: Examples of stoma (a) and non-stoma (b) subimages/regions, which were manually selected and labeled in this work.

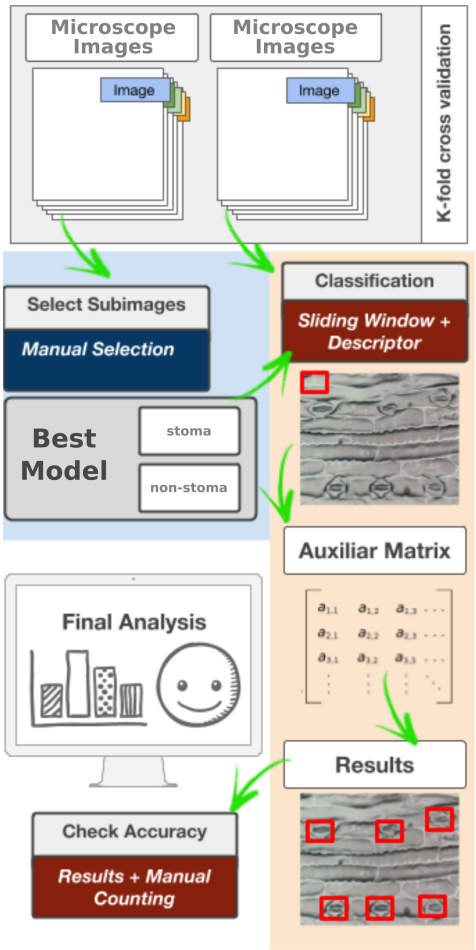

Figure 4: In-depth explanation of the stomata identification process.

4. Experimental Setup

This section describes, in details, the dataset creation process, the technologies, and evaluation protocol used in this work.

4.1. Image Dataset

For optical microscope investigation, it has been necessary to separate the epidermis from the rest of the leaf itself in order to get a clear view of the cell walls and the shape of the stomata [41]. Herein cyanoacrylate glue was applied to the microscope slide in order to obtain

bioRxiv preprint doi: https://doi.org/10.1101/538165; this version posted February 1, 2019. The copyright holder for this preprint (which was not certified by peer review) is the author/funder, who has granted bioRxiv a license to display the preprint in perpetuity. It is made available under aCC-BY-NC-ND 4.0 International license.

an impression of the sheet surface to be captured using a camera attached to a microscope. Leaves were sampled from 20 *Zea mays* cultivars (maize) granted by Nidera Sementes company (UberlndiaMG) producing a total of 200 microscope images with different dimensions such as 2565×3583, 2675×3737, and 2748×3840.

The selected plant species were treated with colchicine [42] in order to change their ploidy and cell morphology for further studies. Due to the plant ploidy specificity, different images might have different stomata sizes and width. Besides, as previously mentioned, stomata differentiation is a process that occurs together with the development of plant organs and herein plants with different ages were used and a clear distinction of the images and plant morphologies can be visualized in Figure 5. In these microscope images, different types of noise might be observed due to many factors which can be seen in Figure 6.

In the experiments, the dataset with 200 microscope images was submitted to the 5-fold crossvalidation protocol, i.e., four parts of the dataset compose the training set (160 images) and one part belongs to the test set (40 images). This process is repeated five times. Therefore, in the stomata classification task, for each microscope image, 5 stoma and 5 non-stoma regions/subimages has been manually select to compose training and test sets in an overall of 2000 subimages.

In the stomata detection task, respecting the separation of the disjoint sets of the 5-fold crossvalidation protocol, each training set created in the stomata classification task is maintained with 1600 subimages. However, the test sets are generated by a sliding window iteration. Hence, for each one of the 40 microscope images existing in each test set, between 876 and 963 regions/subimages are selected by a sliding window iteration resulting in approximately $44,000$ subimages per test set in a overall of $217,866$ subimages for the five runs.

4.2. Programming Environment and Libraries

All the approaches presented in this paper were run on a personal computer with 2.7GHz Intel Core i7-7500U 2.7GHz Intel Core i7-7500U with 16GB of RAM and NVIDIA GeForce 940MX 4GB graphic card. In the same way, the programming language was Python2 with the following libraries: scikit-learn [43], pyleargist, scikit-image[44], opencv [45], keras[46] and tensorflow[47]. A greater part of the libraries were used in order to call image descriptors and deep learning methods.

4.3. Evaluation Protocol

In order to check the accuracy of the created system for classifying and identifying stomata regions, it was used a k-fold cross validation with $k = 5$. The classified images represent the test set and the subimages used to create the learned model were extracted from the training set. A manual count was performed for each image and we evaluated the results using the quantity of identified stomata in selected regions and the total of positive (True Positive) and false classifications (False Positive) using all the generated windows, including the overlapped region results.

5. Results and Discussion

This section shows all experiments performed to validate the proposed system.

5.1. Stomata Classification Task

In this first experiment, we performed a comparative analysis among five image descriptors (HOG, GIST, DAISY, LBP, and Haralick) and three learning methods (Adaboost, MLP, and

bioRxiv preprint doi: https://doi.org/10.1101/538165; this version posted February 1, 2019. The copyright holder for this preprint (which was not certified by peer review) is the author/funder, who has granted bioRxiv a license to display the preprint in perpetuity. It is made available under aCC-BY-NC-ND 4.0 International license.

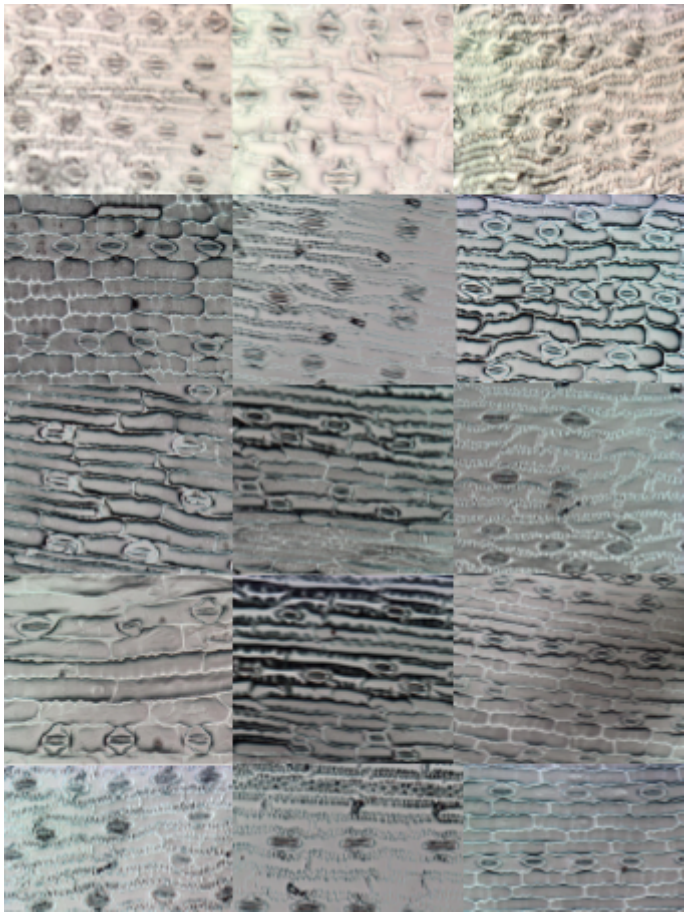

Figure 5: Fifteen different microscope images of Maize Cultivars used in this work.

(a) (b) (c) (d) (e)

Figure 6: Different types of noise present in the microscopic images. (a) the usage of cyanoacrylate glue can generate air bubbles; (b) leaves residuals might be captured by the microscope; (c) the leaves might bend and generate grooves in the image; (d) degradated stomata due to biological factors; and (e) low image quality due to equipment limitations.

SVM) for stomata classification task. All of effectiveness results are measured in mean accuracy of the 5-fold crossvalidation protocol.

As we can observe, in Table 1, the best results have achieved by descriptors purely based on gradient (HOG and DAISY). HOG descriptor with MLP (HOG+MLP) and DAISY descriptor with Adaboost (DAISY+Adaboost) achieved 96.0% of mean accuracy. In a general comparison among all image descriptors, HOG descriptor achieved the best effectivess results with mean accuracy of 94.7% and this can be justified due to the specific shape of the stoma when compared to other parts of the images. Therefore, this fact can show us that shape is the visual property more indicate for the target application. Although GIST is a shape descriptor, perhaps its way

bioRxiv preprint doi: https://doi.org/10.1101/538165; this version posted February 1, 2019. The copyright holder for this preprint (which was not certified by peer review) is the author/funder, who has granted bioRxiv a license to display the preprint in perpetuity. It is made available under aCC-BY-NC-ND 4.0 International license.

of dealing with visual properties globally (holistic) may explain its poor performance in such images.

Table 1: Mean Accuracy of the classifiers based on image descriptor features for stomata classification task.

Learning Method	**HOG**	**GIST**	**DAISY**	**LBP**	**Haralick**
Adaboost	93.0	79.0	**96.0**	88.0	87.0
MLP	**96.0**	81.0	92.0	85.0	80.0
Linear SVM	**95.0**	81.0	80.0	89.0	86.0
Mean	**94.7**	80.3	89.3	87.3	84.3

As the ideal scenario is that all regions are correctly classified in the stomata detection task, another more powerful description approach called deep learning have been performed to improve the effectiveness results achieved by image descriptors.

Table 2 shows effectiveness results of six different deep learning architectures (DenseNet121 – DenseNet, InceptionResNetV2 – IResNet, InceptionV3 – Inception, MobileNet, NasNet, and VGG16) using three learning methods (Adaboost, MLP, and SVM).

Table 2: Mean Accuracy of the classifiers based on deep learning features for stomata classification task.

Classifier	**DenseNet**	**IResNet**	**Inception**	**MobileNet**	**NasNet**	**VGG16**
AdaBoost	95.0	96.0	90.0	96.0	91.0	**99.0**
MLP	98.0	94.0	88.0	98.0	95.0	**100.0**
Linear SVM	80.0	94.0	91.0	98.0	95.0	**100.0**
Epochs	10	13	6	7	16	6
Mean	91.0	94.7	89.7	97.3	93.7	**99.7**

As we can observe, the classifiers based on deep learning features outperformed ones based on image descriptors except for HOG descriptor. In this experiment, the classifiers using VGG16 features achieved the best results with 100% of mean accuracy in almost all three learning techniques performed in this work for stomata classification task.

5.2. Stomata Detection Task

In this experiment, the classifier based on VGG16 features with the support vector machine technique has been adopted for stomata detection task.

Using the sliding window approach for producing possible stoma regions, we have generated between 876 and 963 regions/subimages for each microscope image (overall of $217,866$ subimages) and a 5-fold crossvalidation protocol has been adopted. Each one of these subimages has been labeled using the classifier using support vector machine technique and features generated by VGG16 architecture (SVM+VGG16).

Table 3 summarizes the effectiveness results of the classifier SVM+VGG16. The amount of detected stoma regions are compatible with the manual counting, which shows a good performance of the proposed system. All the 5-fold presented similar effectiveness results with 97.1% of detected stoma regions, i.e., 11388 stomata of the 11734 stomata existing in the dataset.

It is important to comment that the achieved results are better than ones described by [8], which has had an overall of 91.6% of detected regions in the their application.

Once the stomata region candidates have been detected in a microscope image (see Figure 7-(a)), an auxiliary matrix is created through stomata region occurrence (see Figure 7-(b)), a

bioRxiv preprint doi: https://doi.org/10.1101/538165; this version posted February 1, 2019. The copyright holder for this preprint (which was not certified by peer review) is the author/funder, who has granted bioRxiv a license to display the preprint in perpetuity. It is made available under aCC-BY-NC-ND 4.0 International license.

Table 3: Effectiveness results of the classifier (SVM+VGG16) for sliding window classification.

Fold	# Stoma Manual Counting	# Detected Stoma Regions	Total of Regions	# True Positives	# False Positives
1	2244	2189 (97.5%)	43524	5094	107 (0.02%)
2	2374	2300 (96.9%)	43458	5307	159 (0.03%)
3	2428	2316 (95.4%)	43524	5506	153 (0.03%)
4	2279	2213 (97.1%)	43680	5596	60 (0.01%)
5	2409	2370 (98.4%)	43680	5463	49 (0.01%)
Mean	–	2277.6 (97.1%)	–	5393.2	105.6 (0.02%)
Overall	11734	11388	217866	–	–

merge between microscope image and auxiliary matrix is performed (see Figure 7-(c)), and finally, all of stomata are identified in the microscope image (see Figure 7-(d)).

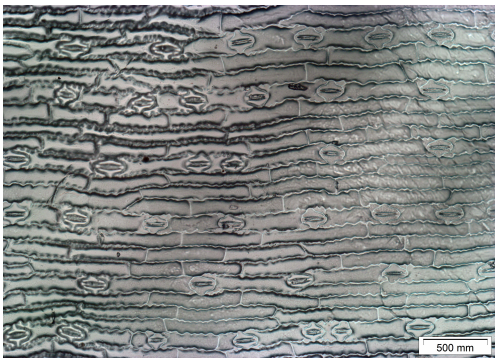

(a) Original microscope image.

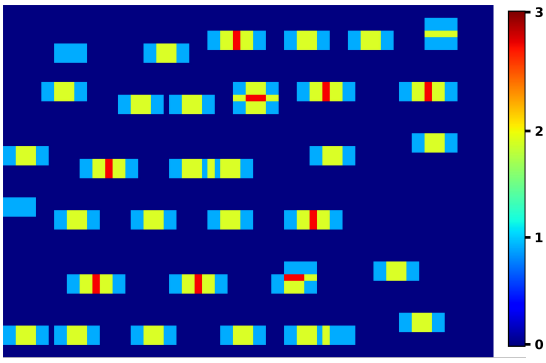

(b) Auxiliary matrix as heatmap.

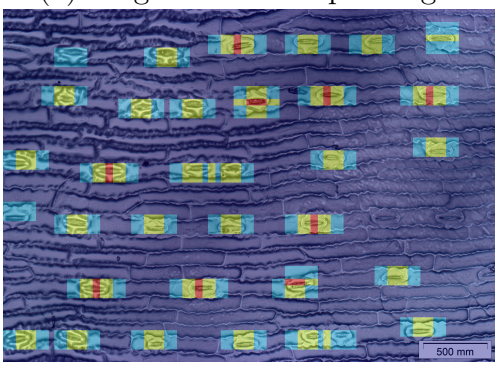

(c) Stomata detection process.

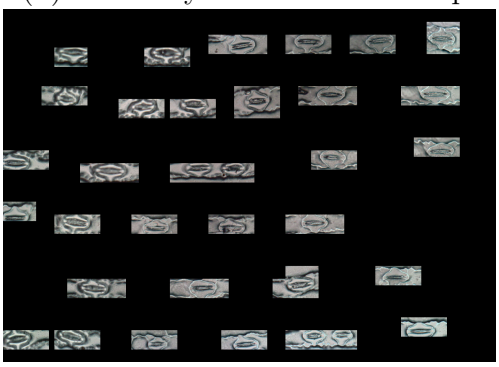

(d) Stomata detection result.

Figure 7: Pos-processing of a microscope image.

As it has been observed in the Table 3, the stomata detection task is not perfect, thus we have analyzed the quality of the effectiveness results. Figure 8 shows the hit and miss classification results achieved by our proposed system.

It is important to observe that regions/subimages with low quality have been also correctly classified as containing a stoma as shown in Figure 8-(a). This fact corroborates the usage of the VGG16 features for stomata detection task. Miss classification can be visualized in Figure 8-(b). Most of these regions/subimages represent plant structures similar to stomata.

bioRxiv preprint doi: https://doi.org/10.1101/538165; this version posted February 1, 2019. The copyright holder for this preprint (which was not certified by peer review) is the author/funder, who has granted bioRxiv a license to display the preprint in perpetuity. It is made available under aCC-BY-NC-ND 4.0 International license.

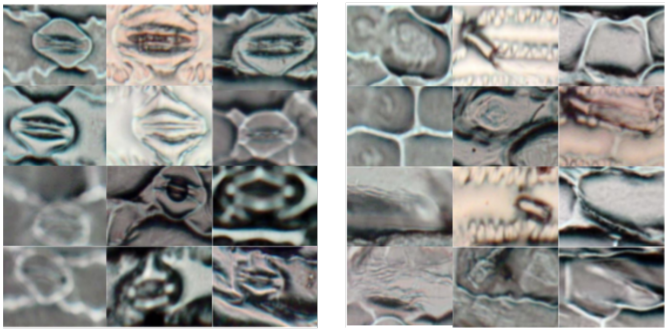

(a) (b)

Figure 8: Examples of the stomata classification results. (a) True positive subimages; and (b) False positive subimages.

6. Conclusion

Leaves microscope images contain relevant information about plant morphology and might be used for studying specific characteristics of metabolic pathways and different biological processes. A vegetative structure that has received more attention is called stoma (in the plural, stomata), which are small pores on the surfaces of aerial parts of most higher plants (e.g., leaves, stems and parts of angiosperm flowers and fruits). Stomata are responsible by many functionality such as (1) exchange of water vapour and CO^2 between the interior of the leaf and the atmosphere; (2) photosynthesis; (3) transpiration stream; (4) nutrition; and (5) metabolism of land plants. Therefore, the understanding of the stomata is of great importance in the exploration of the evolution and behavior of plants.

In this work, we proposed a stomata classification and identification system in microscope images of maize cultivars. Herein we have evaluated different extraction techniques (image descriptor and deep learning) and learning methods (Adaboost, MLP, and SVM) for the task of correctly classifying stomata regions. In this experiments, our approach has achieved mean accuracy of 96% using HOG+MLP and mean accuracy of 100% with VGG16 features using support vector machine (VGG16+SVM).

In the stomata detection task with a sliding window approach for generating all possible regions/subimages from the microscope images, our system has detected 97.1% of the stomata regions existing in the 200 microscope image of the dataset. This fact could show us that our system using deep learning features might be an appropriate solution for target application.

As future work, we intend to develop a computational toolkit to support the specialists on biology area in their research.

Acknowledgement

The authors thanks the support of the Brazilian scientific funding agency CNPq through the Universal Project (grant #408919/2016-7) and the support of NVIDIA Corporation for the donation of the GPUs used for this research.

References

[1] C. Willmer and M. Fricker, *Stomata*. Springer Science & Business Media, 1996, vol. 2.

[2] M. Melotto, W. Underwood, and S. Y. He, "Role of stomata in plant innate immunity and foliar bacterial diseases," *Annu. Rev. Phytopathol.*, vol. 46, pp. 101–122, 2008.

bioRxiv preprint doi: https://doi.org/10.1101/538165; this version posted February 1, 2019. The copyright holder for this preprint (which was not certified by peer review) is the author/funder, who has granted bioRxiv a license to display the preprint in perpetuity. It is made available under aCC-BY-NC-ND 4.0 International license.

[3] A. M. Hetherington and F. I. Woodward, "The role of stomata in sensing and driving environmental change," *Nature*, vol. 424, no. 6951, p. 901, 2003.

[4] H. Meidner and T. A. Mansfield, *Physiology of stomata*. Tata Mcgraw-Hill Publishing Company Limited; Bombay, 1968.

[5] G. Wu, H. Liu, L. Hua, Q. Luo, Y. Lin, P. He, S. Feng, J. Liu, and Q. Ye, "Differential responses of stomata and photosynthesis to elevated temperature in two co-occurring subtropical forest tree species," *Frontiers in plant science*, vol. 9, p. 467, 2018.

[6] M. Melotto, W. Underwood, J. Koczan, K. Nomura, and S. Y. He, "Plant stomata function in innate immunity against bacterial invasion," *Cell*, vol. 126, no. 5, pp. 969–980, 2006.

[7] M. Haworth, C. Elliott-Kingston, and J. C. McElwain, "Stomatal control as a driver of plant evolution," *Journal of Experimental Botany*, vol. 62, no. 8, pp. 2419–2423, 2011.

[8] H. Jayakody, S. Liu, M. Whitty, and P. Petrie, "Microscope image based fully automated stomata detection and pore measurement method for grapevines," *Plant Methods*, vol. 13, no. 1, p. 94, 2017.

[9] C. Hepworth, R. S. Caine, E. L. Harrison, J. Sloan, and J. E. Gray, "Stomatal development: focusing on the grasses," *Current opinion in plant biology*, vol. 41, pp. 1–7, 2018.

[10] J. Vogel, "Unique aspects of the grass cell wall," *Current opinion in plant biology*, vol. 11, no. 3, pp. 301–307, 2008.

[11] K. Omasa and M. Onoe, "Measurement of stomatal aperture by digital image processing," *Plant and cell physiology*, vol. 25, no. 8, pp. 1379–1388, 1984.

[12] P. Sanyal, U. Bhattacharya, and S. K. Bandyopadhyay, "Analysis of sem images of stomata of different tomato cultivars based on morphological features," in *Modeling & Simulation, 2008. AICMS 08. Second Asia International Conference on*. IEEE, 2008, pp. 890–894.

[13] S. Jian, C. Zhao, and Y. Zhao, "Based on remote sensing processing technology estimating leaves stomatal density of populus euphratica," in *Geoscience and Remote Sensing Symposium (IGARSS), 2011 IEEE International*. IEEE, 2011, pp. 547–550.

[14] T. Higaki, N. Kutsuna, and S. Hasezawa, "Lips database with lipservice: a microscopic image database of intracellular structures in arabidopsis guard cells," *BMC plant biology*, vol. 13, no. 1, p. 81, 2013.

[15] K. N. H. S. Higaki, Takumi, "Carta-based semi-automatic detection of stomatal regions on an arabidopsis cotyledon surface," *PLANT MORPHOLOGY*, vol. 26, no. 1, pp. 9–12, 2014.

[16] W. S. Rasband, "Imagej, us national institutes of health, bethesda, maryland, usa," *http://imagej. nih. gov/ij/*, 2011.

[17] N. Kutsuna, T. Higaki, S. Matsunaga, T. Otsuki, M. Yamaguchi, H. Fujii, and S. Hasezawa, "Active learning framework with iterative clustering for bioimage classification," *Nature communications*, vol. 3, p. 1032, 2012.

[18] M. W. da Silva Oliveira, N. R. da Silva, D. Casanova, L. F. S. Pinheiro, R. M. Kolb, and O. M. Bruno, "Automatic counting of stomata in epidermis microscopic images," 2014.

[19] H. Laga, F. Shahinnia, and D. Fleury, "Image-based plant stornata phenotyping," in *Control Automation Robotics & Vision (ICARCV), 2014 13th International Conference on*. IEEE, 2014, pp. 217–222.

[20] F. Awwad, S. Abuqamar, T. Ksiksi, S. Thaker, and A. A. R. Rabee, "Process and device for direct measurements of plant stomata," Jun. 15 2017, uS Patent App. 14/968,954.

[21] K. T. Duarte, M. A. G. de Carvalho, and P. S. Martins, "Segmenting high-quality digital images of stomata using the wavelet spot detection and the watershed transform." in *VISIGRAPP (4: VISAPP)*, 2017, pp. 540–547.

bioRxiv preprint doi: https://doi.org/10.1101/538165; this version posted February 1, 2019. The copyright holder for this preprint (which was not certified by peer review) is the author/funder, who has granted bioRxiv a license to display the preprint in perpetuity. It is made available under aCC-BY-NC-ND 4.0 International license.

[22] E. Tola, V. Lepetit, and P. Fua, "Daisy: An efficient dense descriptor applied to wide-baseline stereo," *IEEE transactions on pattern analysis and machine intelligence*, vol. 32, no. 5, pp. 815–830, 2010.

[23] R. K. McConnell, "Method of and apparatus for pattern recognition," Jan. 28 1986, uS Patent 4,567,610.

[24] M. Douze, H. Jégou, H. Sandhawalia, L. Amsaleg, and C. Schmid, "Evaluation of gist descriptors for web-scale image search," in *Proceedings of the ACM International Conference on Image and Video Retrieval*. ACM, 2009, p. 19.

[25] A. Oliva and A. Torralba, "Modeling the shape of the scene: A holistic representation of the spatial envelope," *International journal of computer vision*, vol. 42, no. 3, pp. 145–175, 2001.

[26] R. M. Haralick, K. Shanmugam *et al.*, "Textural features for image classification," *IEEE Transactions on systems, man, and cybernetics*, no. 6, pp. 610–621, 1973.

[27] T. Ojala, M. Pietikäinen, and D. Harwood, "A comparative study of texture measures with classification based on featured distributions," *Pattern recognition*, vol. 29, no. 1, pp. 51–59, 1996.

[28] T. N. Sainath, A.-r. Mohamed, B. Kingsbury, and B. Ramabhadran, "Deep convolutional neural networks for lvcsr," in *Acoustics, speech and signal processing (ICASSP), 2013 IEEE international conference on*. IEEE, 2013, pp. 8614–8618.

[29] L. Xu, J. S. Ren, C. Liu, and J. Jia, "Deep convolutional neural network for image deconvolution," in *Advances in Neural Information Processing Systems*, 2014, pp. 1790–1798.

[30] S. J. Pan and Q. Yang, "A survey on transfer learning," *IEEE Trans. on Knowl. and Data Eng.*, vol. 22, no. 10, pp. 1345–1359, Oct. 2010.

[31] O. Russakovsky, J. Deng, H. Su, J. Krause, S. Satheesh, S. Ma, Z. Huang, A. Karpathy, A. Khosla, M. Bernstein, A. C. Berg, and L. Fei-Fei, "ImageNet Large Scale Visual Recognition Challenge," *International Journal of Computer Vision (IJCV)*, vol. 115, no. 3, pp. 211–252, 2015.

[32] G. Huang, Z. Liu, and K. Q. Weinberger, "Densely connected convolutional networks," *CoRR*, vol. abs/1608.06993, 2016.

[33] C. Szegedy, S. Ioffe, and V. Vanhoucke, "Inception-v4, inception-resnet and the impact of residual connections on learning," *CoRR*, vol. abs/1602.07261, 2016.

[34] C. Szegedy, V. Vanhoucke, S. Ioffe, J. Shlens, and Z. Wojna, "Rethinking the inception architecture for computer vision," *CoRR*, vol. abs/1512.00567, 2015.

[35] A. G. Howard, M. Zhu, B. Chen, D. Kalenichenko, W. Wang, T. Weyand, M. Andreetto, and H. Adam, "Mobilenets: Efficient convolutional neural networks for mobile vision applications," *arXiv preprint arXiv:1704.04861*, 2017.

[36] B. Zoph, V. Vasudevan, J. Shlens, and Q. V. Le, "Learning transferable architectures for scalable image recognition," *CoRR*, vol. abs/1707.07012, 2017.

[37] K. Simonyan and A. Zisserman, "Very deep convolutional networks for large-scale image recognition," in *International Conference on Learning Representations*, 2015.

[38] B. E. Boser, I. M. Guyon, and V. N. Vapnik, "A training algorithm for optimal margin classifiers," in *Workshop on Computational Learning Theory*, ser. COLT '92, 1992, pp. 144–152.

[39] K. Hornik, M. Stinchcombe, and H. White, "Multilayer feedforward networks are universal approximators," *Neural Netw.*, vol. 2, no. 5, pp. 359–366, Jul. 1989.

[40] R. E. Schapire, "A brief introduction to boosting," in *Proceedings of the 16th International Joint Conference on Artificial Intelligence - Volume 2*, ser. IJCAI'99, San Francisco, CA, USA, 1999, pp. 1401–1406.

bioRxiv preprint doi: https://doi.org/10.1101/538165; this version posted February 1, 2019. The copyright holder for this preprint (which was not certified by peer review) is the author/funder, who has granted bioRxiv a license to display the preprint in perpetuity. It is made available under aCC-BY-NC-ND 4.0 International license.

[41] J. J. Castilloa and M. Ferrarotto, "Evaluation of cyanoacrylate glues for making attached living-leaves epidermis replicas and its scanning electron microscopy observations (evaluación de pegamentos de cianoacrilato para hacer réplicas epidérmicas en hojas vivas adheridas y su observación al meb)," *Scanning*, vol. 20, no. 8, pp. 557–563, 1998.

[42] J. Doležel and P. Binarová, "The effects of colchicine on ploidy level, morphology and embryogenic capacity of alfalfa suspension cultures," *Plant Science*, vol. 64, no. 2, pp. 213–219, 1989.

[43] F. Pedregosa, G. Varoquaux, A. Gramfort, V. Michel, B. Thirion, O. Grisel, M. Blondel, P. Prettenhofer, R. Weiss, V. Dubourg, J. Vanderplas, A. Passos, D. Cournapeau, M. Brucher, M. Perrot, and E. Duchesnay, "Scikit-learn: Machine learning in Python," *Journal of Machine Learning Research*, vol. 12, pp. 2825–2830, 2011.

[44] S. van der Walt, J. L. Schönberger, J. Nunez-Iglesias, F. Boulogne, J. D. Warner, N. Yager, E. Gouillart, T. Yu, and the scikit-image contributors, "scikit-image: image processing in Python," *PeerJ*, vol. 2, p. e453, 6 2014.

[45] G. Bradski, "The OpenCV Library," *Dr. Dobb's Journal of Software Tools*, 2000.

[46] F. Chollet *et al.*, "Keras," `https://keras.io`, 2015.

[47] M. A. et. al., "TensorFlow: Large-scale machine learning on heterogeneous systems," 2015, software available from tensorflow.org. [Online]. Available: `https://www.tensorflow.org/`